

Shallow Reflection Seismics Using Firecrackers as the Source II: Field Experiments

CHIEN-YING WANG¹, RONG-KUAN YANG¹ AND DAO-TZE TSAI¹

(Received 1 July 1991; Revised 20 August 1991)

ABSTRACT

Due to the high resolution requirement of shallow reflection seismics, a firecracker source was invented to generate high frequency signals used in studying shallow structures. Preliminary tests have been done to evaluate its feasibility (Tsai *et al.*, 1991, paper I). Except for a slightly lower energy level, the firecracker source has proved to be efficient, portable, cheap and safe. Its performance was satisfactory. In this paper, a further field test in a good reflection area was conducted to exhibit high frequency signals among the massive noises of groundroll when delineating the underground layers. By setting the geophones at the near as well as the far offset distances, we obtain different but compatible seismic profiles which could provide us with different structural details. Careful and properly adjusted field procedure has always been a key factor for successful shallow seismic reflection studies.

The other purpose of this paper is to use the firecracker source for investigation of near-surface faults whose locations are only grossly known. Three seismic lines, one used in detecting the Hsincheng fault and the other two the Shihtan fault, were shot. They all result in good reflection images illustrating the structural variation across the fault. This kind of near-surface fault mapping provides very detailed information about the fault and the structure, which can be used to understand the faulting processes during the earthquake. It is believed that the developed technique could work equally well for other engineering applications. On account of the outstanding achievements of firecracker source, we may expect a wider acceptance of this powerful method for shallow structure studies in the future.

1. INTRODUCTION

The shallow reflection seismic method has largely been applied to engineering basement investigation, active fault detection and groundwater surveys in the near past years (Steeple and Miller, 1990). Except for smaller survey range (shallower than 500 m), higher signal frequencies (higher than 100 Hz),

¹ Institute of Geophysics, National Central University, Chung-Li, Taiwan, R. O. C.

and simpler field survey procedures, the reflection seismic method used in shallow structure study does not differ much from that used in large scale oil exploration (Wang *et al.*, 1991). Knapp and Steeples (1986 a,b) successfully detected several near-surface faults using the Common Depth Point (CDP) reflection survey technique, including the Meers fault (Myers *et al.*, 1987) and the Borah peak fault (Treadway *et al.*, 1988). Their studies attracted considerable attention to the use of this high resolution geophysical method in investigating fine and detailed shallow structures.

Due to the necessity of high frequencies for shallow seismics, we have invented a tool which detonates a firecracker to provide a sharp seismic source. The designation and the properties of this firecracker source have been described in Tsai *et al.* (1990) (referred to as Paper I) which is the first part of this research sequence. Except for a slightly lower energy level, the firecracker source has been demonstrated to be a convenient source possessing the properties of efficiency, portability, low cost and safety. The present paper will concentrate on the field performance of this newly developed source used for generating high frequency signals to overcome the groundroll noise and in fault detection. Two topics will be included. The first discusses the problem of groundroll suppression by sharp high frequency signals created with this firecracker source. It is to evaluate the upper limit that the firecracker source can express. The other topic will study cases of active fault detection. Two faults are under consideration: the Hsincheng fault and the Shihtan fault. These two faults have been extensively studied using other methods, thus providing a framework to measure the performance of our shallow reflection method. It is hoped that the discussion will give us a deeper view of shallow reflection seismics and help to promote the method as applied in solving problems of shallow structure studies.

2. GROUNDROLL SUPPRESSION EXPERIMENT

Sufficient high frequency signals have been obtained from the firecracker source as illustrated in paper I. Using this source, we have been able to work under many different conditions. In this section, an experiment for the suppression of groundroll using high frequencies will be discussed. It could test the limit of high frequency generation from the firecracker source.

It is known that the shallower the target to be detected, the closer the geophone spread and the higher the frequency that is needed for shallow reflection seismics (Steeple and Miller, 1990). However interference due to air-wave noise and groundroll largely degrades the signal exhibition for near offset geophones (Figure 1). These noises have very large amplitude and long duration which nearly "flush" the useful reflection signals. There exist two methods to "battle" with the groundroll noise, i.e., to "avoid" or to "conflict" with the

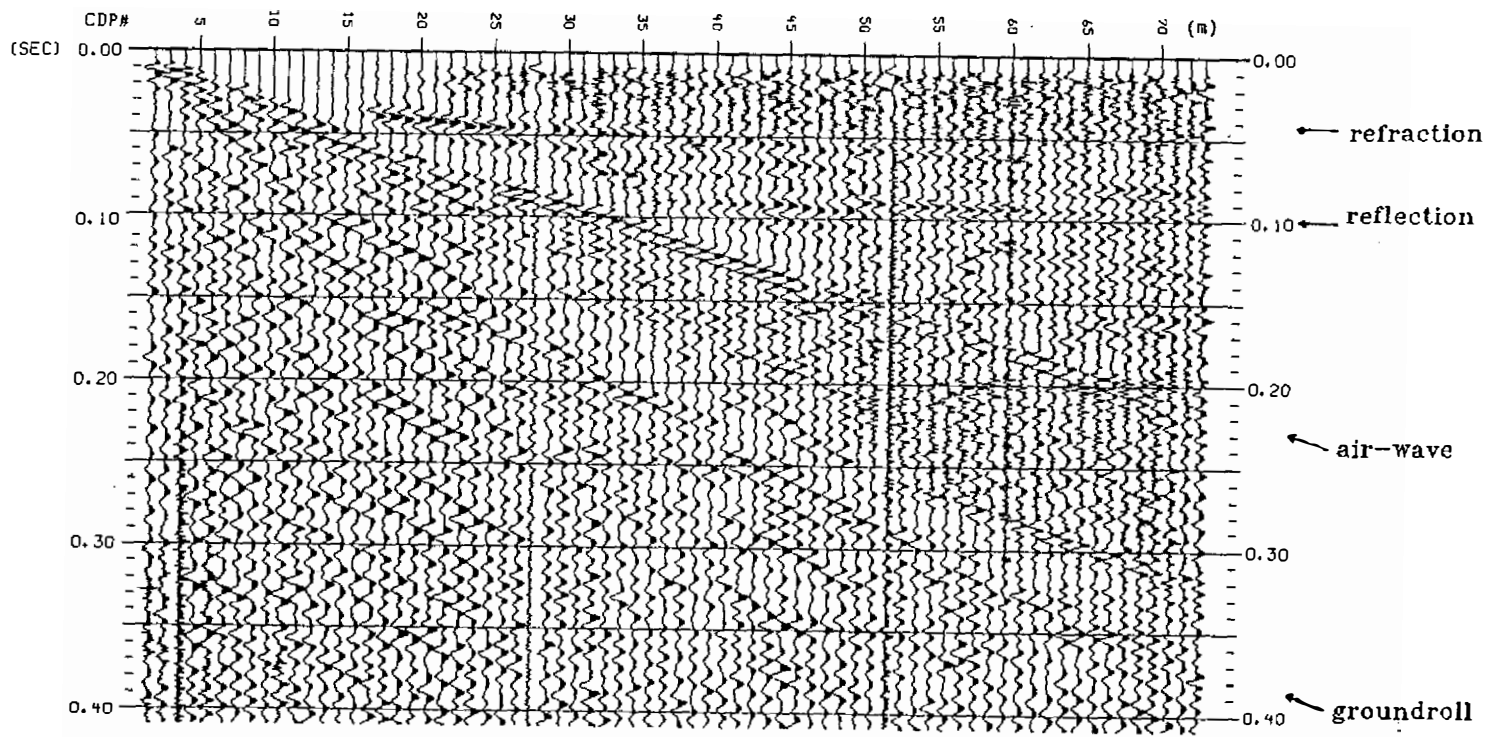


Fig. 1. Section of a walkaway noise test conducted at the survey area in Figures 2~5. The geophone interval is 1 m and three 24-channel geophone spreads accomplish the section. A 100 Hz low-cut pre-emphasis filter of seismograph and 100 Hz geophones are used. Each trace has only been applied with a 40 msec AGC before plotting. Different types of signals and noises are indicated. The groundroll appears to be the biggest noise which needs to be overcome in the shallow seismic reflection study.

groundroll. The "avoidance" method uses the low velocity property of the groundroll (smaller than 300 m/sec) by setting the receivers at large offset distances which collect the reflection signals before the arrival of the groundroll flood. This distance range is called the "optimum window" by Pullan and Hunter (1985). The "avoidance" method, however, suffers from the problems of weak signal due to the long travel distance, wide-angle reflection and NMO stretch if data processing is imposed. On the other hand, the "conflicting" method uses the low frequency property of the groundroll (lower than 50 Hz), setting the receivers at short offset distances and the recording system to high frequencies to delete the groundroll noise before it enters the system. Except for high frequency sources, geophones, and recording instruments, the "conflicting" method largely depends on the ground conditions which will transmit high frequency signals. Unfortunately, it seems not to be always the case for most surveys. Both the "avoidance" and the "conflicting" methods have their advantages and shortcomings. Which method is more capable is still a big debate in shallow seismic reflection studies (Pullan *et al.*, 1991).

To distinguish the characteristics of the "avoidance" and the "conflicting" methods, we designed the following experiments:

Experiment I: geophone interval 2 m , near-trace offset 40 m , low-cut filter 100 Hz .

Experiment II: geophone interval 1 m , near-trace offset 6 m , low-cut filter 200 Hz .

The test site of the experiment is a cropped rice field. The ground is pretty wet which helps geophone coupling and wave transmission. A Geometrics ES-2401 24-channel seismograph and OYO 100 Hz geophones are used. The firecracker source is shot 4 times at each station. Every station contains a shot, thus producing a 12 fold CDP section. The collected data is processed using the SSS system developed by our research group as described in Paper I or Wang *et al.* (1991). New generation computer workstations (HP9000-835S and HP9000-730) have greatly promoted the performance of this system.

Figure 2 and Figure 3 display the shot records obtained in Experiments I and II, respectively. In each of these figures, (b) is the case of (a) after proper data processing which includes frequency filter, dip filter, and a 40 msec AGC. Experiment I (Figure 2) has a large offset distance, its geophones are distributed over a wider range ($40\text{ m} \sim 86\text{ m}$) to receive the signals before the groundroll arrivals which are mostly restricted at the low-left corners of the profiles (see Figure 2a). The survey area has good reflectors that are even visible down to 400 msec (about 450 m deep). However the region of the section where the groundroll prevails lacks useful signals even after data processing. Figure 3 (Experiment II), on the contrary, has a shorter geophone interval

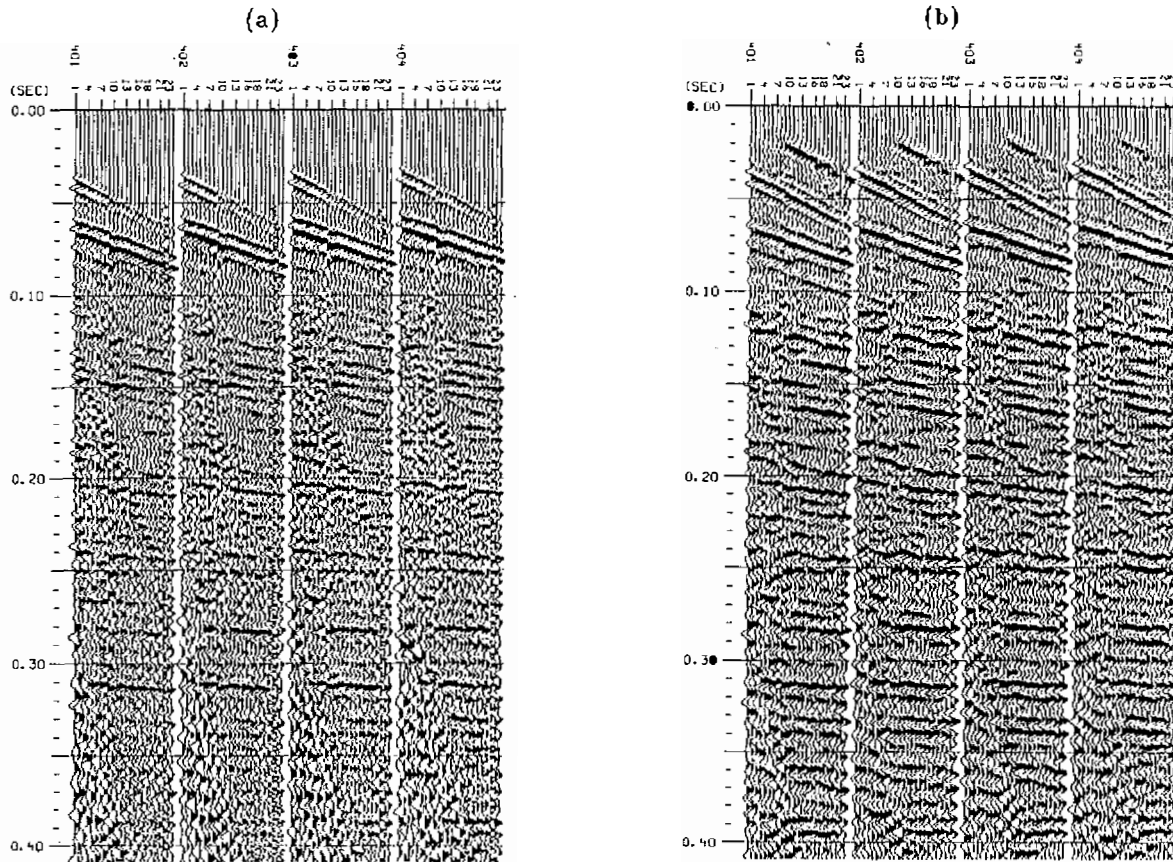


Fig. 2. The shot records of groundroll suppression experiment I. (a) is the original record and (b) is the record after proper data processing. File numbers are denoted at the upper-left corner for each record. A geophone interval of 2 m and a near-trace offset of 40 m are used in this experiment. It is apparent that the groundroll noises are restricted at the low-left corner of each shot record. We call this the "avoidance" method of groundroll suppression. Strong reflection events are still standing on at the time below 200 msec.

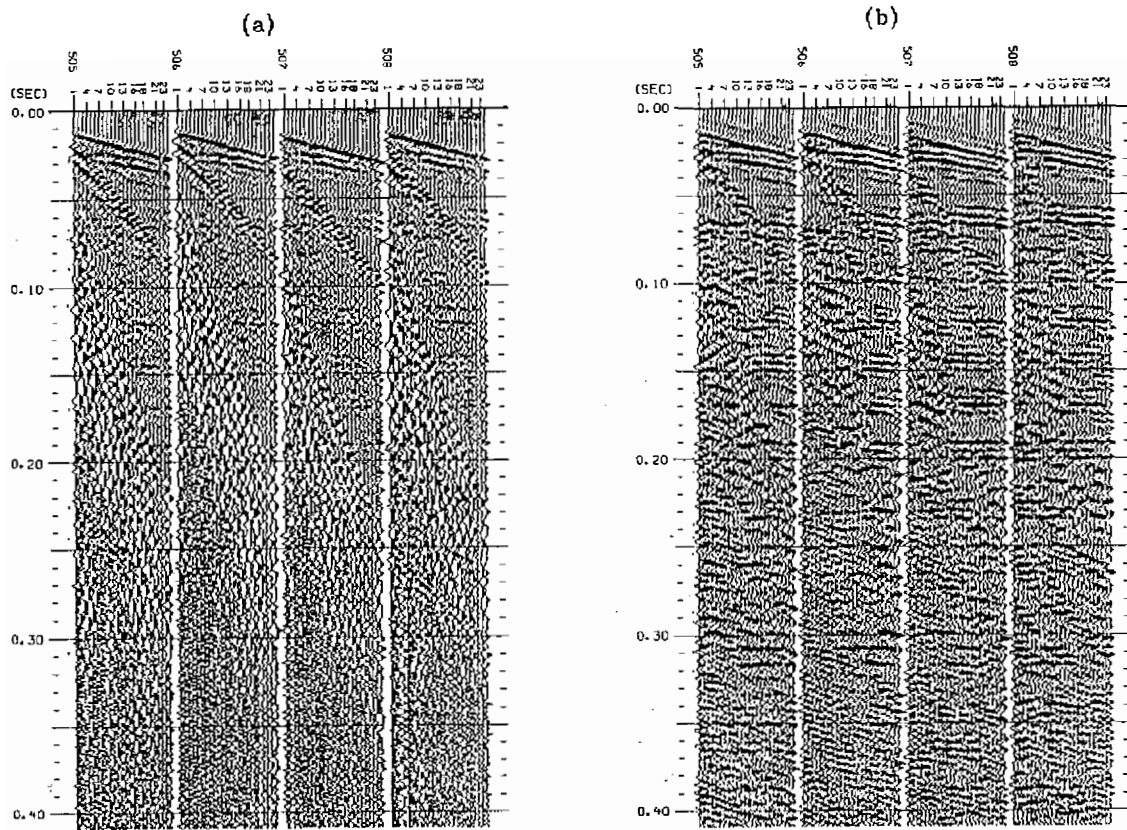


Fig. 3. The shot records of groundroll suppression experiment II. The display is similar to Figure 2. A geophone interval of 1 *m* and a near-trace offset of 6 *m* are used in this experiment. A 200 *Hz* low-cut pre-emphasis filter has been set during data collection. The groundroll noises are suppressed (penetrated) and the reflection events float out only after data processing as seen in (b). We call this the “conflicting” method of groundroll suppression. Good coherent signals are visible above 200 *msec*, but below this the events become weak due to lack of high frequency energy after the long travel distance.

(1 *m*) and near offsets (6 *m* ~ 29 *m*). It uses a higher low-cut pre-emphasis filter (200 *Hz*) to suppress the groundroll noises before they are recorded through an AD convertor of the seismograph. Although Figure 3a is full of air-wave and groundroll noises, it becomes much clearer (Figure 3b) after signal enhancement by data processing. Good reflection signals "penetrate" the area of groundroll noises as those indicated around 150 *msec* and 200 *msec* arrival time. This is apparently a result of high frequency signal preservation after groundroll suppression. However, the signals below 200 *msec* become obscure due to the low energy level of the high frequencies able to reach there. Figure 4 shows the frequency content of one of the files plotted in Figures 2a and 3a. It is apparent that Experiment II has much higher and wider frequency content than Experiment I. Thus higher resolution power should be attained for Experiment II. There are some abnormal signals in top 30 *msec* of Figure 2b and Figure 3b, which are caused by imperfect trim of front ends after dip filter.

Figure 5 shows the final stacked seismic sections. Figure 5a is for Experiment I and 5b for Experiment II. The part of the section in Figure 5a where Experiment II was taken is also indicated. For ease of layer identification, Figure 5b was redrawn in Figure 5c with a lighter color and the interpretation superimposed. Experiment II (Figure 5b) has much better structural resolution than Experiment I, a consequence of high and wide frequencies, but its section is still polluted by the groundroll noise. The reflection signals are lost below 100 *msec* especially on the low fold part at both sides of the section. Nevertheless, Experiment I (Figure 5a) possesses good structural layering due to stronger reflection events over the whole section. The events between 220 *msec* and 270 *msec* of Experiment I are not resolved well as compared to Figure 5b. This could be due to wide angle reflection disturbance or multiple reflections of the thin layers. One other important thing worth pointing out is the first event at 25 *msec*. It is doubtful at first glance whether the first arrivals in Figures 2 and 3 are "refraction" signals. If they were, they should be muted (Steeple and Miller, 1990). By conducting a refraction survey along the same profile using a sledge hammer and 30 *Hz* geophones, we have identified good refraction arrivals with an intercept time of 5 *msec* (equivalent to 1.5 *m* depth). After considering this, the first event in Figure 5 could correspond to a reflection signal from a layer below the 1.5 *m* deep weathering layer boundary. It is said that the event at 25 *msec* of the sections should not be a refraction, but may represent the shallowest reflector (might be at 5 *m* deep) the method can detect. Wilson (1990) has used model study of shallow seismic data to examine the behavior of head waves. He strongly suggested neglecting of head waves in shallow seismic reflection due to their small amplitudes (only 10% of reflections) especially at large offsets. We have come to the same conclusion in this experiment.

The above groundroll suppression experiments express different empha-

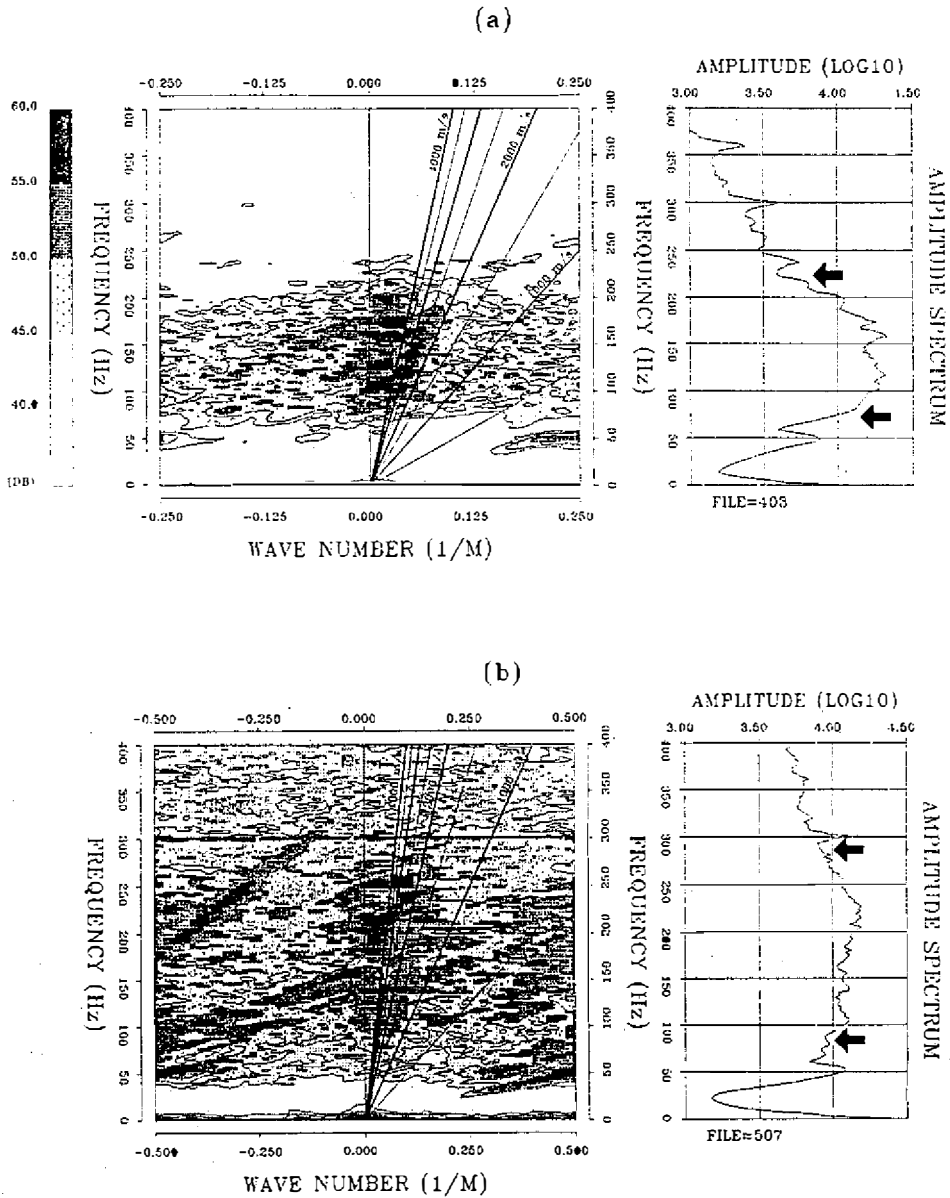


Fig. 4. A comparison of frequency content for unprocessed signals from experiment I (a) and II (b) as shown on Figures 2a and 3a, respectively. A 40 msec AGC has been applied before the $f - k$ analysis. The file numbers are also indicated. From the distribution of signals above the 1500 m/s apparent velocity on $f - k$ plot, we may identify the useful signals and their frequency range (indicated by arrows on the amplitude spectrum). (b) has higher and wider frequencies than (a), which may result in a higher resolution on the time section. This figure also indicates the fact that frequencies of 230 Hz (from (a)) and 300 Hz (from (b)) are attainable using the firecracker source.

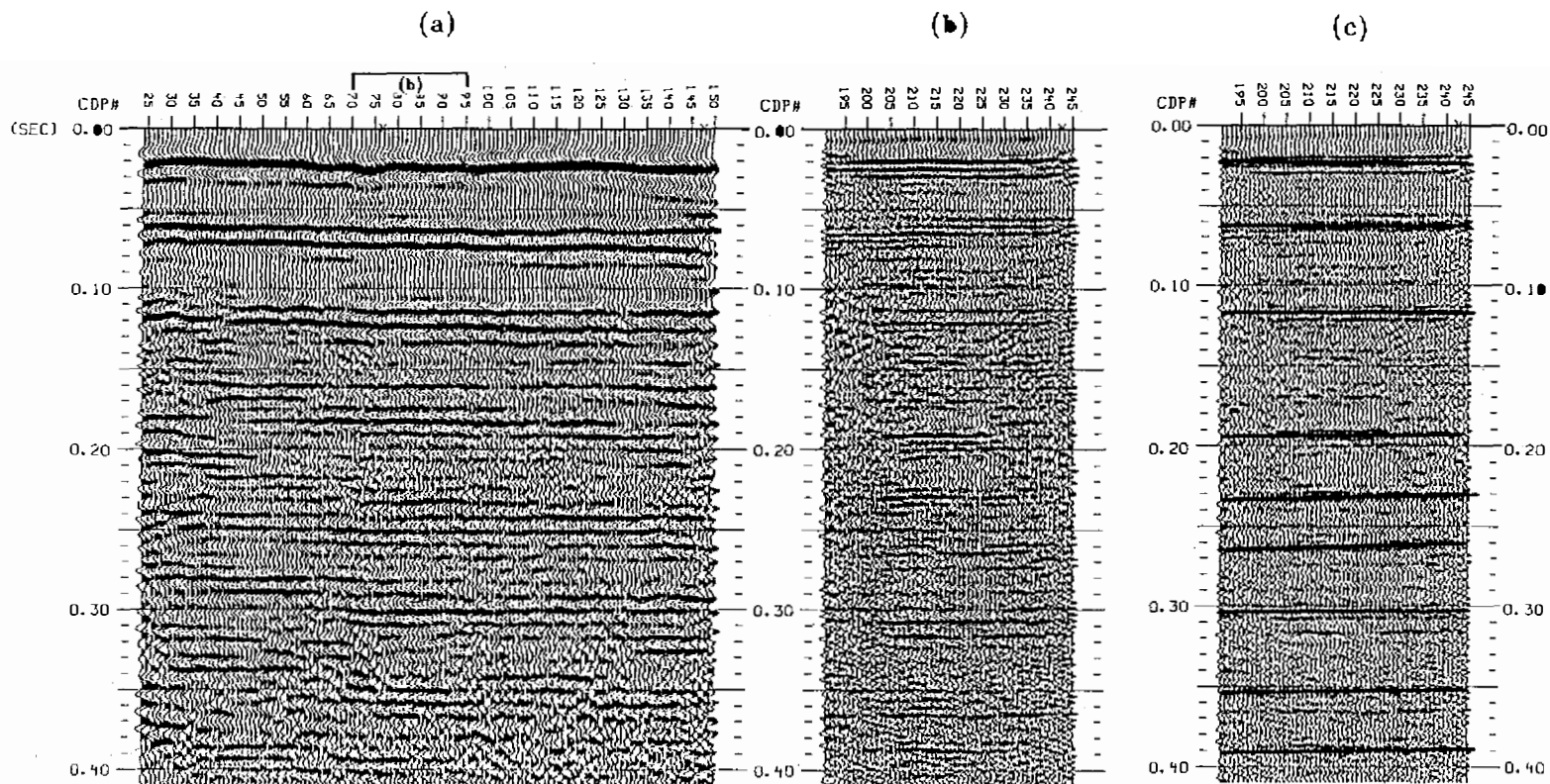


Fig. 5. The final stacked seismic sections of the groundroll suppression experiments. (a) is for experiment I, (b) is for experiment II, and (c) is a display similar to (b) except for a lower amplitude and with interpretation. See text for detail explanation.

sized points for shallow reflection surveys. If a very shallow target were wanted, a short distance and high frequency should be used, otherwise, a far offset (at least 30 *m*) is a better choice to expose deep reflections before the interruption of groundroll. Steeples and Miller (1990) have mentioned running two surveys along the same line if reflections were needed for the full depth range (both above and below 20 *m*). It does not seem possible to obtain complete information of underground structure from 0 *m* to 500 *m* by a single survey. This is a significant point worthwhile of consideration by the user who is going to apply the method.

From the above experiment, the firecracker source was again proved to be eligible and convenient. Incorporating the proper field procedure and data processing, the system established by the firecracker source should be capable of accomplishing most tasks. In the next sections, we will discuss more cases of fault detection.

3. FAULT DETECTION

3.1. Hsincheng fault

3.1.1. Geological condition and field work

The Hsincheng fault is located in Hsinchu county, northwestern Taiwan. It is a thrust fault which has a length of about 18 *km* in a NE-SW direction and dips 40° SE. The inferred Hsincheng fault trace lies in a region between axes of the Chintsohu anticline and the Paoshan anticline. The rocks in the SE part of the fault are mainly sandstone/mudstone interlayers of Pliocene Cholan formation, while those in the NW part are mainly massive sandstone and sandstone/mudstone interlayers with intercalated thin conglomerate layers of Pleistocene Toukoshan formation. The southeastern block has been thrust over the northwestern block during fault action. Some studies showed that the Hsincheng fault displaced not only Pleistocene lateritic terrace deposits but also recent non-lateritic deposits, and suggested that the Hsincheng fault was once reactivated along the old fault plane (Hsu, 1986, p.92). It may be categorized as "potentially active fault" (reactivated before Pleistocene, but not recently).

The rocks on both sides of the Hsincheng fault are not much different (Huang, 1984), and the fault traces can hardly be seen on an air-photo map (Tang, 1968). As a result of the development of the Chintsohu and Paoshan gas fields with detailed geological studies in this area, the existence of Hsincheng fault has already been assured. Ten fault outcrops were reported by Huang (1984), and he also indicated that the fault displacement near the surface is about 15 *m*, and the fault zone may be as wide as 30 *m* in some areas. The seismic survey area is located just between the first and the second western Taiwan highway.

The survey line is located near Ta-Chi village, Hsinchu, as to be shown in Figure 7d. The line strikes NS and the measurements were taken along a roadside. As extended from the field topography analysis, the survey line runs approximately perpendicular to the Hsincheng fault (Figure 7d). The field work took 8 days to complete two seismic lines. The first line with a length of 300 *m* is directed south to north and the second line, 200 *m*, is in the reverse direction from north to south using the same station positions as the first line. These two reversed lines were shot in order to verify the reliability of data reciprocity and repetition in shallow reflection seismics. The same seismograph, geophones, and field display parameters as for groundroll suppression experiment I discussed in the above section were used. The seismograph was set using a 100 *Hz* low cut filter to suppress the low frequency groundroll. A small hole of about 50 *cm* depth was prepared for the firecracker source, which was filled with water to improve the energy release.

Figure 6 displays a sample of the field record and its frequency-wavenumber analysis. This record was obtained with the source at $x = 22$ *m* and the receivers between $x = 82$ *m* and 128 *m*. Since the geophone interval, dx , equals 2 *m*, the distance along the survey line is supposed to be the same as the CDP# (defined as shot location# + receiver location# - 1). This is the reason we frequently use the CDP# in our seismic section display (e.g., Figure 5). By checking with the final stacked section (Figure 7a), we feel that the diffraction pattern appearing on Figure 6a at channel# 9 and 19 could be real (Kanasewich and Phadke, 1988) which may be due to the effect of fault discontinuity. The available frequencies are found to be between 80 *Hz* and 220 *Hz* from Figure 6c. This may resolve the layers with a thickness of about 3 *m* (Knapp, 1990).

3.1.2. Data Processing and final sections

The collected shot records were first elevation corrected, then passed through a 90 ~ 220 *Hz* bandpass filter and a 50 *msec* window length AGC. These were used to suppress the low-frequency groundroll and to balance the amplitude of the record. In order to further remove the groundroll and air-wave noises, we chose a dip filter by passing the events with a velocity higher than 800 *m/sec*. The dip filter enhances the reflection events, but it may also cause false signals when the record contains large random noises. Care should be taken when using this filter. We also tested the deconvolution filter, but its effect is quite limited. This is probably due to the uneven signal wavelets on each record. The shallow seismic data usually does not have a high enough signal-to-noise ratio, which makes successful decon difficult to obtain.

The treated shot records are next sorted into CDP gathers. Velocity analysis is then performed on several of the CDP gathers. A constant velocity

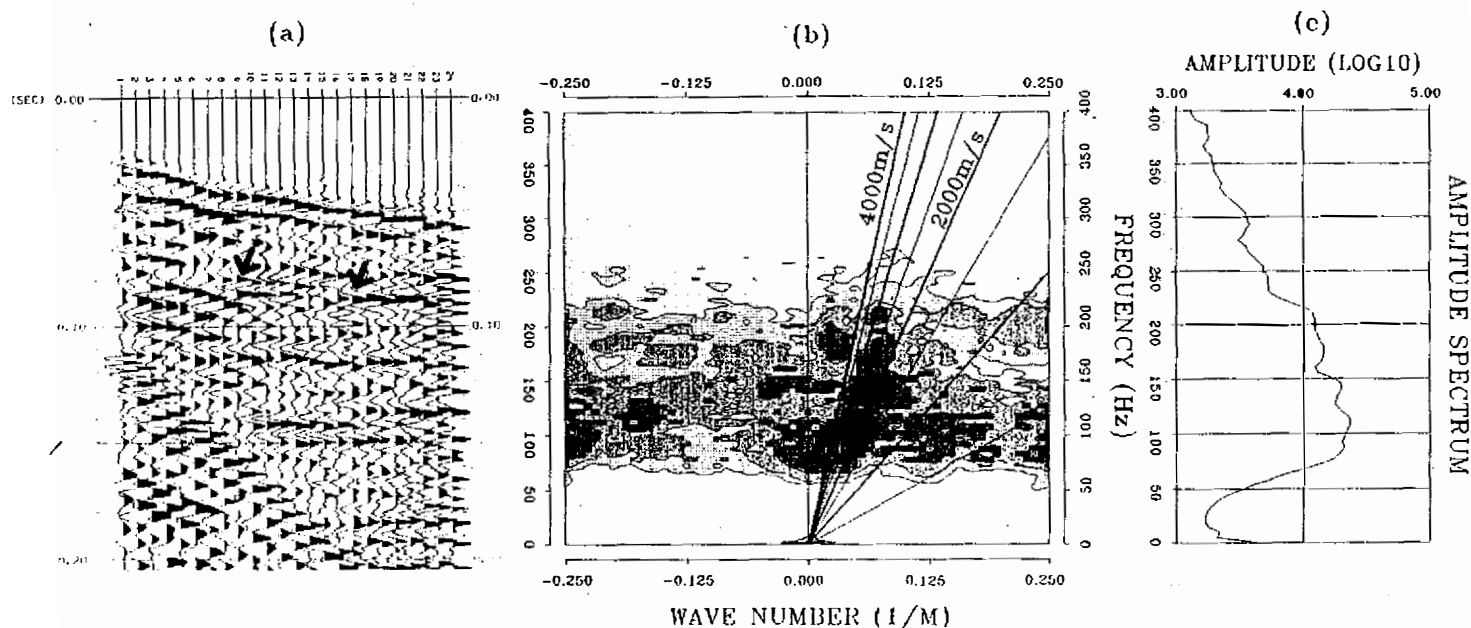


Fig. 6. A shot record from the firecracker source detecting the Hsincheng fault. (a) is the shot record, (b) is its $f-k$ analysis, and (c) is the average amplitude response. Different events including the reflection signals (nearly flat events) and the noises (mostly at the low-left corner) are presented in (a). The slant lines in (b) correspond to the apparent velocities varying from 500 m/sec to 4000 m/sec with an increment of 500 m/sec . The source is at $x = 22 m$ and the receivers are between $x = 82 m$ and $128 m$. These x 's distances have the same number as the CDP number shown on Figure 7 due to the fact $dx = 2 m$. Some diffraction patterns shown around channels 9 and 19 indicate the effect of faulting.

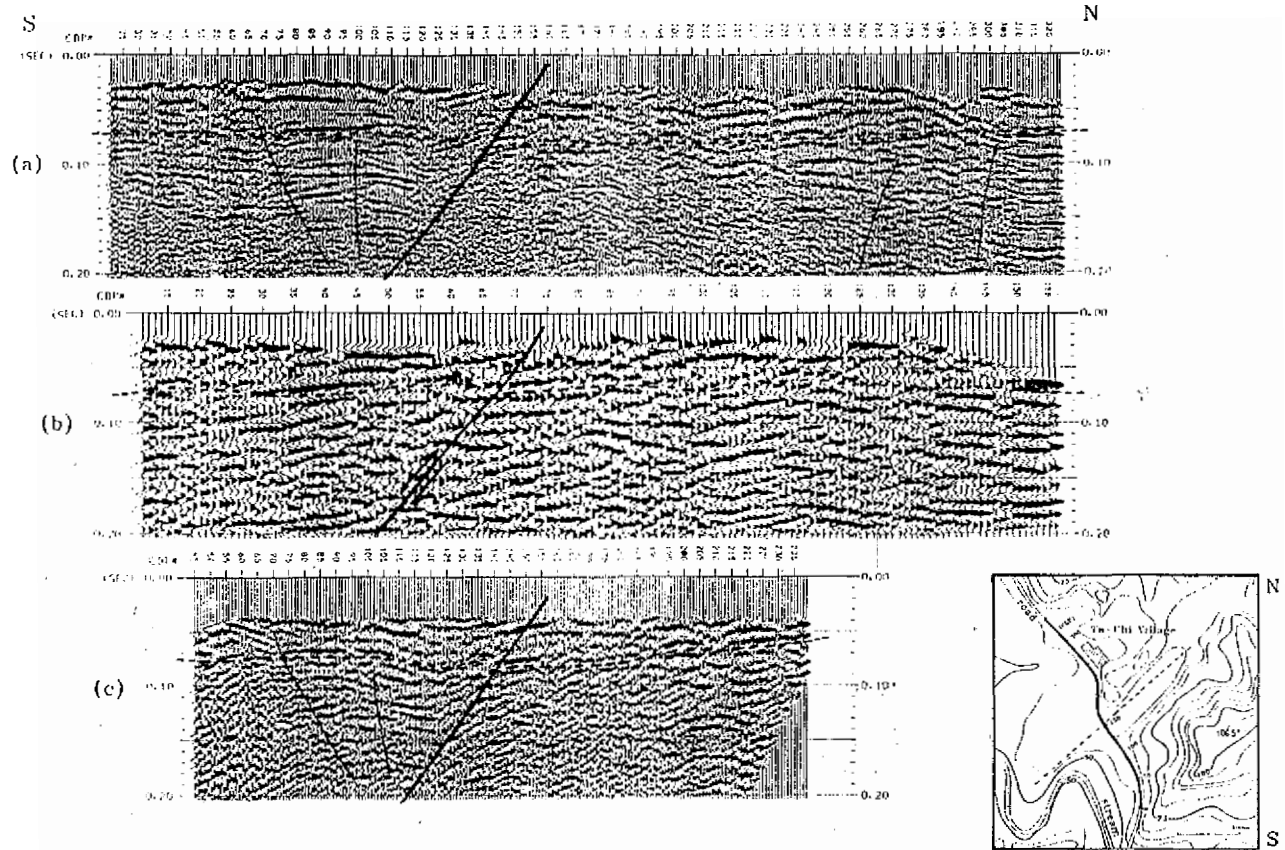


Fig. 7. The final seismic sections for the Hsincheng fault detection. (a) is for the northward seismic line, (b) is for the dynamite source, (c) is for the southward line, and (d) is a scratched map of the survey area. The fault location is determined by carefully comparing (a) with (c). (b) is too coarse for this purpose. A basically smoothed layer (dashed line) above 100 msec for the part with CDP# larger than 150. However the events between CDP# 70 and 150 vary widely. Some buckling and fracture are apparent on the upper block of the fault due to the thrust movement from the south.

scan (CVS) and/or velocity panel is taken to reveal the velocities which stack the data better after NMO shifting. By choosing various velocities along several CDP's (usually 20 CDP interval each), we then NMO and stack the section which further passes through a filter before resulting in the final seismic section.

Figure 7 shows the final stacked sections of the Hsincheng fault. Figure 7a is for the northward directed seismic line, 7c is for the southward directed line, and 7b is a previous result from Yang and Guo (1991) which was obtained using a Dynasource impact source and 4 m geophone spacing. Section 7b is included only for comparison. Theoretically, the results of these three sections should be equivalent due to the reciprocal and repetitive properties of seismic wave propagation. However, the reality comes out as not so ideal. It can be seen from Figure 7a that the reflection events are obscure between CDP# 130 and CDP# 200 (CDP interval is 1 m). We may separate the section into three parts, front, middle, and last according to these two CDP locations. The front and the last part of the survey line are along a hill (Figure 7d) which has consolidated sandstone present. The middle part is beside a rice field and the surface is soft. The geophone coupling is not good there. From the surface topography, it is quite reasonable to assume that the fault may be located in the middle region.

After carefully comparing Figures 7a and 7c, we can determine the faults as those drawn on the figures. But Figure 7b (from Dynasource) is too coarse for this purpose. Its frequency content is low (lower than 70 Hz), although some event coherencies are visible as compared to Figures 7a and 7c. The high frequency signals are of importance in detecting the fault from this comparison. By examining these figures, we can found a major fault accompanying with several front wall breakages. The sense of movement on the fault plane is indicated in Figure 7b (south side upthrust). The events under CDP #80 and #110 have obviously different trends showing broken layers offset by faults. This may represent a buckling and twisting fracture on the hanging wall of a reverse thrust fault under great horizontal compressive stresses. Several times of faulting are visible from different fault slips at different depths or places of the section. An average fault offset distance of 20 m on the figure seems a good estimate agreeing well with field observations (Huang, 1984).

3.2. Shihtan fault

3.2.1. Shihtan earthquake fault history and field work

The Shihtan fault was caused by 1935 Hsinchu-Taichung Earthquake ($M = 7.1$), the biggest damage earthquake (3279 casualties and 17907 houses destructed) in Taiwan history. The earthquake is very shallow (10 km or 5 km, Miyamura, 1985) and its epicenter is located near to the present Liyutan dam site, Maoli. To refresh the memory of this large on-land earthquake, a fifty-year

memorial ceremony was held in Apr. 20, 1985. A special issue was published after this activity (see reference of Miyamura, 1985).

Due to the intensive investigation of field rupture and damage by the Japanese, who occupied Taiwan at that time, valuable earthquake fault details were reported (Otuka, 1936). The earthquake fault consists of (1) a right lateral strike-slip fault (called Tuntzuchio fault) trending N60E with a maximum horizontal displacement of more than 1 *m* and vertical displacement of less than 60 *cm* in the southwestern wing of the epicenter, (2) a dip-slip reverse fault (called Shihtan fault) trending N30E with a maximum of 3 *m* uplift on the west side relative to the east side without appreciable horizontal displacement in the northern wing of the epicenter. The Shihtan earthquake fault has a total length of 15 *km* and dips 70 ~ 80° W. Bollina (1977) summarized the active faults in Taiwan and also touched on the 1935 earthquake, although the "Chihhu" fault as he called it instead of the "Shihtan" fault which is now regularly used by the researchers in Taiwan. Folds in this area consist of northeast-trending anticlines and synclines with axial reverse faults. The Shihtan earthquake fault occurred in an overturned bed called "Shangfuchi sandstone" that makes up the eastern limb of the Chihhu syncline and the western limb of the Pakuali anticline. The Shangfuchi sandstone belongs to the late Miocene Nanchuang formation, which is coarse grained, uncompacted and seems easily reshaped under stress. Most structural layers in this area are near vertical.

Two earthquake fault scarps are still visible today (Pan, 1983). One is located 1.5 *km* east of Bai-Sou village (new name of Chihhu) and the other is at Sun-Ta-Wer village. Two seismic lines are designed near these two scarps, which are named line I and II, respectively. The topography maps of the survey lines can be seen in Figures 9b and 10b. The object of this investigation is to explore the ability of seismic method to detect active faults near a fault whose position is grossly known.

The seismic field work was done during the rainy winter season. We feel that the seismic signals behave better on the wet ground surface, which are probably in favor of wave propagation due to water's assistance. The field parameters for line I include a 1.5 *m* geophone interval, a 20 *m* near-trace offset and a 100 *Hz* filter, for line II, a 2 *m* geophone interval, a 40 *m* near-trace offset and a 100 *Hz* filter. Line I is on an abandoned farm field whose surface condition is much better than line II which is along a country road. Figure 8 shows examples of field records from line I. Figure 8a was obtained with the shot at location #1 and the receivers between #14 and #37. Figure 8b was from the shot at location #4 and the receivers between #17 and #40. The fault trace is expected to be around location #23 (i.e., CDP #45 in Figure 9). Some event discontinuity and diffraction pattern (marked by a gray color in Figure 8) appear on these records near the predicted fault location. This is a

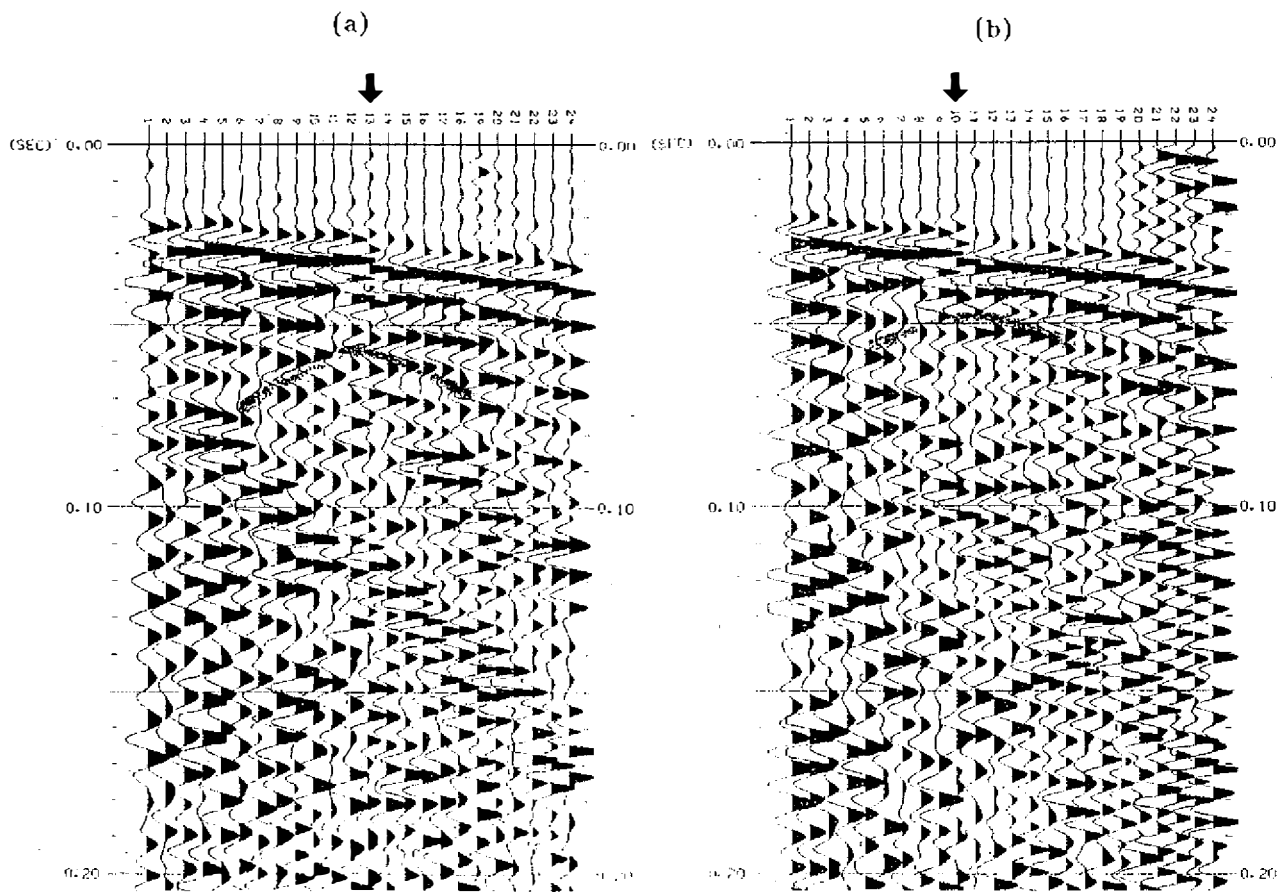
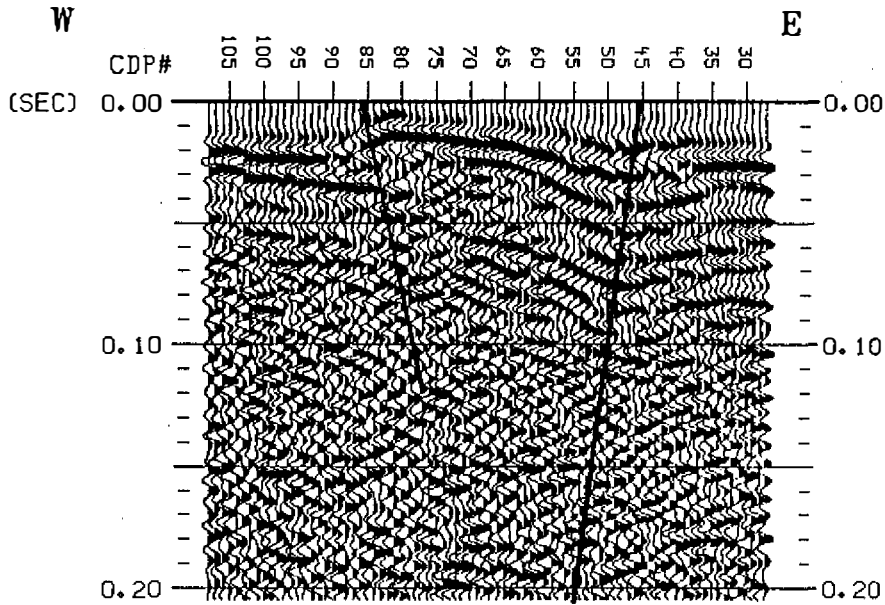
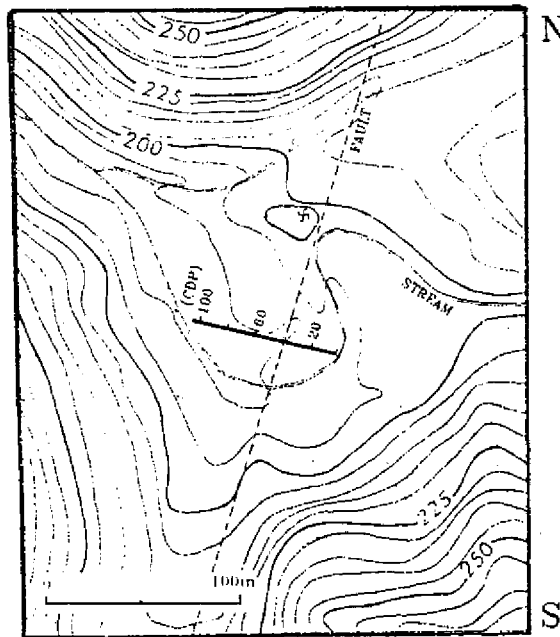


Fig. 8. Two shot records from the Shihtan seismic line I. (a) is obtained with the shot at the location #1 and the receivers at locations between #14 and #37. (b) is obtained with the shot at #4 and the receivers between #17 and #40. The fault scarp is expected to be at location #23 (i.e. CDP# 45). Some event discontinuity and diffraction patterns appear on these records. This is a good indication of the effects of a near-surface fault on shallow reflection records.



(a)



(b)

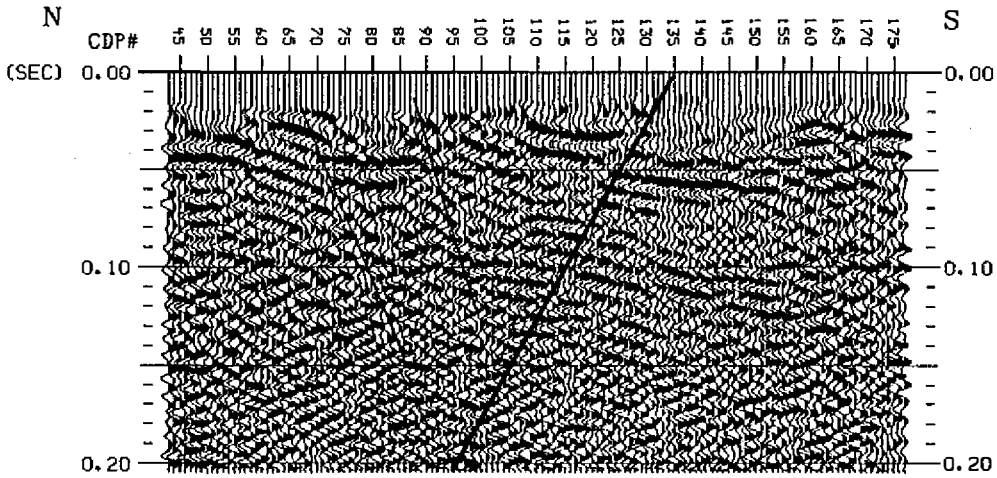
Fig. 9. The final seismic section (a) and the scratched survey area map (b) of the Shihtan seismic line I. Note that the hill where a Landblesser Shrine is situated was formed during the earthquake. A 5 m height was uplifted which blocked the stream and made it change its flow direction. The seismic section depicts a very good picture of the fault which agrees surprisingly well with the surrounding landscape.

good indication of faulting on original reflection records, and those may produce a fault image finally on the stacked section (Figure 9). The frequency content of the record is found to be as high as 200 *Hz*.

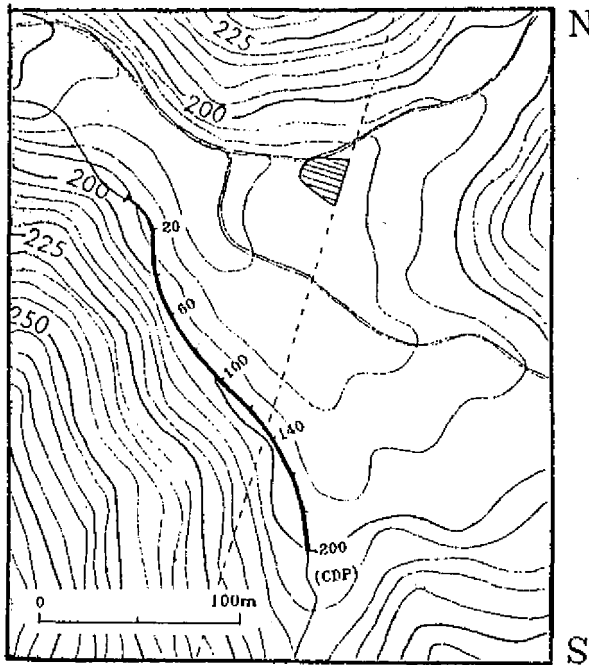
3.2.2. Final sections

Figure 9a shows the final stacked section of line I. A scratched map of the survey area is also illustrated on Figure 9b. It is noticed that the hill on which a Landblesser Shrine is situated was formed during the earthquake. A 5 *m* high outcrop was uplifted which blocked the stream and made it change its course shown as a curve in Figure 9b. The seismic section (Figure 9a) depicts a very good picture of the fault which agrees surprisingly well with the surrounding landscape. The mass between CDP #45 and #85 seems to be pushed up and clutched by faults on two sides. The fault on the east side has a drag type which is supposed to correspond to the main fault with appreciable structural distortion and the fault on the west side appear to be a clear rupture. The mass uplifted has relation with a highly dipping layer of Shangfuchi sandstone which is coarsely glued and easy to collapse by the pressure due to earthquake action. It seems that the soft Shangfuchi sandstone is squeezed and flows out to push the overlying alluvial layers and makes them distorted. The reflection events below 70 *msec* are not presented due to high layer dip angles of the surrounding deep structure. However, the near-surface layers have revealed unambiguous fault image in this case.

Figure 10a shows the final seismic section for line II and Figure 10b depicts the map around the studied area. A landmass upheaval 3 *m* high, 25 *m* wide and 40 *m* long caused by the earthquake is indicated by the shaded area in Figure 10b. The seismic section, 100 *m* away from the land upheaval, reveals an apparent fault image whose location is just at the line extended from the fault scarp (CDP #135 in Figure 10a). Similar fracture types as in Figure 9 are seen, which may represent the squeeze effect of faulting on the coarse grained, uncompacted Shangfuchi sandstone in which the earthquake fault grew. It is not unreasonable to assume that the whole length of the Shihtan fault having relation with this soft sandstone layer. It took the burden of the structural deformation under large earthquake fault stresses. The apparent dip of the main fault in Figure 10a is less than that in Figure 9a. This may be due to the oblique crossing of the seismic line with the fault strike. A wider rupture zone is occupied in line II and the fracture process may have caused larger structural disturbance. This could be a good example showing earthquake deformation to the near-surface structures.



(a)



(b)

Fig. 10. The final seismic section (a) and the scratched survey area map (b) of the Shihtan seismic line II. A landmass 3 m high, 25 m wide and 40 m long was uplifted by the earthquake (indicated by the shaded area in (b)). The seismic section which is 100 m away from the fault outcrop reveals apparent faulting on the section which is located just along the fault line (dashed line in (b)). Similar fracture types as in Figure 9 exist which may represent the squeeze effect of the earthquake fault happening in a coarse grained, uncompacted Shangfuchi sandstone.

4. DISCUSSION AND CONCLUSIONS

This paper discussed two cases using firecracker sources for a shallow seismic reflection study; one is used to suppress groundroll noises by isolating high frequency signals and the other for fault detection. These cases provide a good evaluation to check the performance of firecracker source. The results are quite satisfactory. The seismic images obtained are surprisingly good which are uneasy to obtain by other methods. The tests give us tremendous confidence for the developed method.

The firecracker source can generate sufficiently high frequencies (upto 300 Hz). By incorporating proper survey procedures, it can be used in delineating very shallow and fine structures after proper suppression of groundroll noises for the near offset spread. However, structures below 30 m should be detected using wider receiver offsets. The conditions under which to choose the right "optimum window" are still big questions. More work needs to be done in this respect.

The Hsincheng fault is identified in the seismic sections. The quality of data obtained from this survey was not good. However, by shooting two reverse lines, we still have an opportunity to narrow down the possible fault location. An important benefit of the seismic method is its direct, unambiguous indication of structure. By repeating the survey, the desired signals may gradually float up as being proved in this study.

The seismic survey for the Shihtan fault detection is also a successful example. The clear seismic picture of underground structure makes it easy to explain faulting procedures during the earthquake. It can be thought of as a result of squeezing a soft sandstone formation in which the fault developed. The match of the structure determined with the surface landscape nicely confirms this explanation. This experiment further proves the feasibility of firecracker source seismics.

Although the cases studied all give positive results, in our experience, however, the success of the method strongly depends on the field work. A proper choice of space window and frequency window to receive most useful signals and reject noises is continuously a challenge. A noise test cannot be skipped even for familiar circumstances. The CDP technique is certainly of help to improve the signal-to-noise ratio. The fold number it produces had better higher than 12 in order to leave us chances to select better traces used in stacking process.

The depth studied in this paper is between 20 m to 200 m . We may need higher frequency sources such as a shotgun for much shallower structure determination (smaller than 30 m , Miller *et al.*, 1986). It requires a higher frequency source for shallower structures. The experience accumulated in this

paper, however, is of great help in promoting our technique. On account of the outstanding performance made by firecracker source, we may expect a wide application of this powerful geophysical method in solving problems of shallow structure investigation in the future.

Acknowledgements. The authors wish to express their sincere attitude to Dr. Yang, Chieh-Hou and his student Mr. Guo, Tai-Rong for allowing us to use their data in the Hsincheng case comparison study. We also thank many students of SSS group, especially Ms. Shyu, Li-Wen, Ms. Jiang, Yu-Yan, Mr. Jong, Tai-Tong and Mr. Wu, San-Cheng, who assisted the field work. This research was supported by the National Science Council under grant NSC80-0414-P008-04B and the Central Weather Bureau under grant CWB81-2E-6.

REFERENCES

- Bollina, M. G., 1977: Summary of quaternary faulting and elevation changes in Taiwan, *Mem. of Geol. Soc. of China*, **2**, 43-55.
- Huang, C. S., 1984: Quaternary faults in the coastal area between Hsinchu and Chunan, north-western Taiwan, *Special Publication of Central Geological Survey*, **3**, 103-126.
- Hsu, T. L., 1986: *Geology and Engineering*, 2nd ed., Ker-Chi Book Company, Taipei (in Chinese).
- Kanasewich, E. R. and S. M. Phadke, 1988: Imaging discontinuities on seismic sections, *Geophys.*, **53**, 334-345.
- Knapp, R. W., 1990: Vertical resolution of thick beds, thin beds and thin-bed cyclothem, *Geophys.*, **55**, 1183-1190.
- Knapp, R. W. and D. W. Steeples, 1986a: High-resolution common depth point seismic reflection profiling: instrument, *Geophys.*, **51**, 276-282.
- Knapp, R. W. and D. W. Steeples, 1986b: High-resolution common depth point seismic reflection profiling: field acquisition parameter design, *Geophys.*, **51**, 283-291.
- Miller, R. D., S. E. Pullan, J. S. Waldner and F. P. Haeni, 1986: Field comparison of shallow seismic sources, *Geophys.*, **51**, 2067-2092.
- Miyamura, S., 1985: The Hsinchu-Taichung, Taiwan, Earthquake of April 20, 1935. in: *Special Issue for the Fifty-year Memorial Ceremony of 1935 Hsinchu-Taichung Earthquake*, Central Weather Bureau, Taipei.
- Myers, P. B., R. D. Miller and D. W. Steeples, 1987: Shallow seismic-reflection profile of the Meers fault, Comanche County, Oklahoma, *Geophys. Res. Letters*, **15**, 749-752.
- Otuka, Y., 1936: The earthquake of Central Taiwan (Formosa), April 21, 1935. in: *Papers and Reports on the Formosa Earthquake of 1935*, Bull. of the Earthq. Res. Inst., Tokyo.
- Pan, K. L., 1983: *Analysis of 1935 Hsinchu-Taichung Earthquake fault using remote sensing, geological, and geoelectrical data*. Report to the National Science Council, NSC, Taipei (in Chinese).
- Pullan, S. E. and J. A. Hunter, 1985: Seismic model studies of the overburden-bedrock reflection, *Geophys.*, **50**, 1684-1688.
- Pullan, S. E., R. D. Miller, J. A. Hunter and D. W. Steeples, 1991: Shallow seismic reflection surveys: CDP or "Optimum Offset?". Presented at the 61th Ann. Internat. Mtg., Soc. Explor. Geophys., Houston, abstracts and biographies, 469-471.

- Steeple, D. W. and R. D. Miller, 1990: Seismic reflection methods applied to engineering, environmental, and groundwater problems. in: S. H. Ward (ed.). *Geotechnical and Environmental Geophysics, Vol. I: Review and Tutorial*, SEG publication, Tulsa, USA.
- Tang, C. H., 1968: Photogeological observation on the low hilly terrain and coastal plain area of Hsinchu, Taiwan, *Petro. Geol. Taiwan*, **6**, 71-79.
- Treadway, J. A., D. W. Steeples and R. B. Miller, 1988: Shallow seismic study of a fault scarp near Borah Peak, Idaho, *J. Geophys. Res.*, **93**, 6325-6337.
- Tsai, D. T., C. Y. Wang and R. K. Yang, 1990: Shallow reflection seismics using firecrackers as the source, I: firecracker source, *TAO*, **1**, 307-320.
- Wang, C. Y., C. H. Hsieh, D. T. Tsai and L. W. Hsu, 1991: Experiences with the shallow reflection seismics as applied to the shallow structure study, *Proc. Geol. Soc. China*, **34**, 111-130.
- Wilson, T. H., 1990: Model studies of shallow common-offset seismic data, *Geophys.*, **55**, 394-401.
- Yang, C. H. and T. R. Guo, 1991: Geophysical study of Hsincheng fault, Hsinchu, Taiwan. Presented at: The Third Taiwan Symposium on Geophysics, (Exp. Abs.).

爆竹震源淺層反射震測 第二部份 野外測試

王乾盈 楊榮堃 蔡道賜

國立中央大學地球物理研究所

摘要

本研究第一部份已說明爆竹震源之設計、特性及其使用之情形。除了能量稍弱以外，爆竹震源可說是效率高、容易攜帶、價廉及安全。本文（本研究第二部份）主要探討爆竹震源震測在野外之實際表現。我們選擇一個反射極佳的地區，研究爆竹震源產生高頻之能力，及其用在克服地面波之一些方法，結果顯示爆竹震源結合不同的施測方式，可有效的展示地下不同部份之構造。審慎的施測將可獲得符合目的的震測剖面。

本文另一目的為使用爆竹震源來偵測三個已知的活斷層：一個為新城斷層，另二個用於探測獅潭斷層。三個震測剖面皆表現出清晰的斷層影像及其附近之地層構造。該震測結果與地表地質所決定的斷層位置，極為吻合，其所提供之詳細地下構造變化，亦可用來瞭解地震斷層之作用。

本研究明白指出爆竹震源淺層反射震測之發展潛能，該法被廣泛應用於解決各種淺層構造之問題，將是指日可待的事。